Journal of Applied Fluid Mechanics, Vol. 19, No. 4, pp. 811-830, 2026.
Available online at www.jafmonline.net, ISSN 1735-3572, EISSN 1735-3645.
https://doi.org/10.47176/jafm.19.4.3918

Design and Transient Flow Characteristics of New Differential Large Flow Safety Valve

N. Li[1†], X. Yang[1], S. Wang[2], G. Zhao[1], and Y. Song[3]

[1] *Liaoning Technical University, School of mechanical engineering, Fuxin, Liaoning, China*
[2] *Nanjing Ye Hengda Intelligent System Co., Ltd, Nanjing, Jiangsu, China*
[3] *YingKou Institute of Technology, School of Mechanical and Power Engineering, Yingkou, Liaoning, China*

†*Corresponding Author Email: 47221016@stu.lntu.edu.cn*

ABSTRACT

This paper presents a novel differential-type high-flow safety valve, with a rated flow and pressure of 3000 L/min and 50 MPa respectively, aimed at enhancing the impact resistance and stability of hydraulic supports. Based on the Ansys Fluent platform, dynamic mesh technology and User-Defined Functions (UDF) were employed to identify the optimal damping hole radius for the differential high-flow safety valve. The transient fluid characteristics throughout the opening process until stable unloading were simulated for valves featuring damping hole radii of 1 mm, 2 mm, and 3 mm. Based on the optimal damping hole radius, test samples were developed high flow safety valves and constructed a rapid dynamic loading shock test rig to evaluate their shock resistance characteristics. Results indicate that a damping hole radius of 2 mm achieves the best overall performance in both transient response characteristics and operational stability. The differential high-flow safety valve demonstrates rated flow and pressure of approximately 2996 L/min and 49.4 MPa respectively, with valve core opening time of under 2 ms, unloading time of under 5 ms, and pressure overshoot of below 20%. These findings validate the structural rationality of the differential high-flow safety valve and confirm its advantages in rapid unloading speed and excellent impact resistance.

Article History

Received August 21, 2025
Revised November 8, 2025
Accepted November 14, 2025
Available online February 5, 2026

Keywords:

Hydraulic support
Differential large flow safety valve
Dynamic grid technology
User-defined functions
Rapid dynamic load impact test

INTRODUCTION

Comprehensive mechanized mining not only enhances coal production but also significantly reduces labor requirements, improves working conditions for underground personnel, and provides stronger safety safeguards. It represents the fundamental pathway toward achieving safe, efficient, and environmentally sustainable coal mining. The mechanical equipment in comprehensive mining faces primarily consists of "three machines" (coal cutters, hydraulic supports, and scraper conveyors), which form the essential foundation for high-efficiency and safe coal extraction (Duan et al., 2022). During underground operations, reliable support at the working face serves as both a fundamental and critical condition for coal mining. Thick coal seams account for 43% of China's total coal reserves, making thick coal seam mining with comprehensive mechanized technology a key competitive area in global coal production. As mining faces advance deeper into rock masses, discontinuous surrounding rock structures become prevalent (Shan et al., 2024). When the equilibrium between coal seam and rock mass forces is disrupted, the energy released exceeds its consumption, leading to rockburst phenomena (Ren et al., 2023). Rockburst occurs suddenly and destructively, releasing massive energy that primarily impacts hydraulic supports. To ensure working face safety and stability, it is crucial to enhance the structural strength and rigidity of hydraulic supports while improving auxiliary components' performance to mitigate impact forces (Xiangpeng et al., 2023).

In hydraulic support systems, valve components serve as critical auxiliary elements whose operational reliability directly impacts the system's load-bearing capacity and safety margins (Zhao et al., 2020). As one of the three primary control components in hydraulic supports, the safety valve acts as a vital overload protection mechanism. Its primary function is to regulate the actual working resistance within permissible limits. The valve remains closed during stable support operations, with its sealing integrity ensuring the airtightness of the pillar circuit control system (Xiangpeng et al., 2023). With

NOMENCLATURE

A_1	flow area of safety valve outlet	ρ	density of working medium
A_z	flow area of damping hole	K_1	spring curvature coefficient
a_t	spring helix angle	L	spring extension length
C	spring winding ratio	n_1	effective number of spring turns
C_d	flow coefficient	P_0	pressure at safety valve outlet
d	diameter of inlet	P_{max}	maximum set pressure of safety valve
d_1	small diameter of differential chamber	Q_g	rated flow of differential safety valve
D_1	diameter of main valve core	R	radius of damping hole
F_1	working load of spring	S_z	bonding area between damping hole and cavity
f_1	deformation under spring working load	t	spring pitch
g_g	gravitational acceleration	V_g	flow velocity at valve seat inlet
H_0	free height of spring	X_0	maximum displacement of main valve core
α_1	half-angle of valve core cone angle	x_z	axial overlapping distance
γ	water's gravitational force		

the continuous advancement of coal mining technologies, increased mine depths, and expanding extraction areas, these developments have raised higher performance and stability requirements for hydraulic supports. As an indispensable key component in coal mine hydraulic systems, the safety valve's performance directly determines the technical specifications of the entire support system. Conventional mine safety valves can no longer handle significant load impacts, necessitating the development of high-flow safety valves to overcome limitations in high-pressure and high-flow environments (Zeng et al., 2024). To achieve this, while maintaining structural simplicity, reliable sealing, and operational stability, continuous improvements in dynamic performance are essential to enhance the system's ability to respond to sudden load variations. This ultimately elevates the support performance of hydraulic supports and ensures safe production in mines.

Chiavola et al. (2022) designed a hydraulic damper to reduce safety valve failure rates by addressing operational instability issues such as noise and premature wear. Through validation of safety valves with different damper configurations (from no damping to strong damping), they analyzed how damper layout affects pressure overshoot and stabilization time, thereby verifying the effectiveness of dampers in cone valve safety systems (Chiavola et al., 2022). Burhani and Hős (2021) conducted static and dynamic simulations for direct-acting spring-loaded safety valves under two-phase (water-air) non-impulse flow conditions. Simulation results revealed that fluid dynamics coefficients and flow coefficients at the valve port vary with fluid mass fraction and valve lift (Burhani & Hős 2021). Ajitabh Pateriya et al. performed finite element analysis using ANSYS Workbench software on direct-acting relief valve materials. Finesso & Rundo (2017) investigated the influence of safety valve core geometry on pressure-flow characteristics, establishing a three-dimensional transient simulation model in ANSYS Fluent. Through dynamic mesh configuration and user-defined functions (UDFs) to simulate fluid flow interaction with core motion, they predicted pressure-flow dynamic characteristic curves under different spring preload settings and core structures. Comparative analysis between simulation results and experimental data revealed close agreement, ultimately determining the optimal cone angle for the core based on experimental findings (Finesso & Rundo 2017). Dasgupta & Karmakar (2002) analyzed single-stage relief valves with damper units (consisting of dampers, baffles, and springs). Before simulation, they linearized the valve's mathematical equations and simplified its 3D model. Transient response results validated that damper units could mitigate core motion amplitude during valve unloading, with physical principles explaining the reliability of this phenomenon (Dasgupta & Karmakar 2002). Kim et al. (2018) employed the "Characteristic Method" from multi-objective genetic algorithms to conduct forward transient analysis and optimization of linear-action safety valve parameters—spring stiffness, compression, and valve body mass. Comparative analysis showed optimized valves exhibited reduced core vibration amplitude and frequency levels. Okabe et al. (2019) investigated cavitation phenomena in pure water hydraulic slide valves by creating transparent acrylic resin models for visualization. Through vibration and noise measurements with varying gas volume fractions, they found that larger valve orifice openings resulted in smaller gas volume fractions and consequently reduced noise levels (Okabe et al., 2019). Hos et al. (2014) coupled overflow valve dynamics with one-dimensional pipe gas dynamics, conducting experiments on three common linear overflow valves under varying flow rates and pipe lengths. Their results showed intense oscillations in all valve cores, though those in the longest pipeline exhibited minimal vibration, revealing that core instability correlates with effective orifice area and pipe length (Hős et al., 2014). Couzinet et al. (2014) utilized ANSYS CFX to simulate shear stress transfer in three-dimensional overflow valve models, performing URANS simulations. They applied the Rayleigh-Plesset model to predict cavitation during valve unloading, proposed modifications to saturated vapor pressure in cavitation models to account for turbulent effects, and established flow visualization models to evaluate hydraulic performance impacts of flow coefficients during safety valve unloading (Couzinet et al., 2014). Filo et al. (2021) conducted research on the flow characteristics of relief valves and methods to reduce pressure loss. Using CFD simulation software, they modified the geometry of the relief valve flow field model to identify the geometric configuration with the lowest flow resistance. By establishing a physical relief valve based on the flow field model and conducting experimental verification, they found that the relative error between CFD simulation results and experimental data

was no more than 6%, confirming the accuracy of the simulation results .

As a critical auxiliary component in hydraulic support column circuit control systems, the dynamic characteristics of safety valves directly determine the operational efficiency, stability, and safety of these systems (Zhao et al., 2020). With the continuous increase in coal mining depths, hydraulic supports now face growing external load impacts and higher frequency shock effects (Morselli et al., 2019), necessitating enhanced performance requirements for column circuit control systems. Compared to direct-acting and pilot-operated safety valves, differential safety valves demonstrate superior pressure regulation precision, responsive sensitivity, and reliable sealing performance. These advantages make them particularly suitable for high-pressure, high-flow applications in column circuit control systems.

1. STRUCTURE AND WORKING PRINCIPLE OF DIFFERENTIAL LARGE FLOW SAFETY VALVE

1.1 Differential Large Flow Safety Valve Structure

The differential compact safety valve primarily consists of key components including the main valve core, valve sleeve, sleeve cylinder, valve seat, spring, and spring seat. Given its compact structure, the sealing system employs a space-efficient O-ring dynamic seal mechanism (Sharma et al. 2023). To ensure optimal response sensitivity and sealing reliability, a conical sealing configuration is adopted. To optimize the valve core's motion characteristics, a damping-regulating conical throttle valve is installed at the left end of the main valve core's central bore, effectively suppressing high-frequency vibrations during unloading phases. The structural design of the differential large-flow safety valve is illustrated in Fig. 1.

1.2 Working Principle of Differential Large Flow Safety Valve

When the hydraulic support is subjected to external load impact, the column begins to gradually descend to maintain constant working resistance. The internal working medium in the cylinder body is compressed, causing a sudden pressure surge in the column circuit control system. When the system pressure reaches the differential high-flow safety valve's opening pressure threshold, high-pressure working fluid directly acts on the main valve core 7 through port 4 of the valve seat. The main valve core 7 moves axially to the right under hydraulic pressure. A portion of the high-pressure fluid flows into the differential chamber through the conical throttle valve's damping hole 8 and the main valve core's damping hole 11, generating leftward hydraulic pressure that counteracts the rightward force from the inlet. This creates a differential effect. Upon opening, the safety valve's main valve core 7 rapidly discharges high-pressure fluid from port 1 of the valve sleeve, swiftly reducing system pressure to protect both the column circuit control system and the hydraulic support against impact. During the unloading process, the compressed working medium causes localized deformation in the cylinder body. The released energy leads to a pressure rebound, moving the main valve core 7 axially to the right again. Throughout the unloading phase, the safety valve's main valve core 7 maintains continuous axial movement until the internal pressure drops below the safety valve's opening pressure, prompting its timely closure.

Compared with the direct-acting safety valve, the differential safety valve has a differential chamber in the valve body. The hydraulic pressure generated by the differential chamber can offset part of the pressure impact of the inlet, which effectively alleviates the hydraulic impact of the inlet under the same working conditions and reduces the performance requirements on the safety valve spring (Zha et al., 2024).

2. KEY STRUCTURE AND PARAMETER DESIGN OF DIFFERENTIAL LARGE FLOW SAFETY VALVE

The rated flow of the differential large flow safety valve is 3000 L/min, the rated pressure is 50 MPa, and the working medium is high water based liquid.

2.1 Valve Seat Structure Design

The schematic diagram of the seat structure of the differential large flow safety valve is shown in Fig. 2.

The theoretical formula for the inlet diameter is:

$$d \geq \sqrt{4\times 16.67 Q_g / 100\pi V_g} = 0.463\sqrt{Q_g / V_g} \tag{1}$$

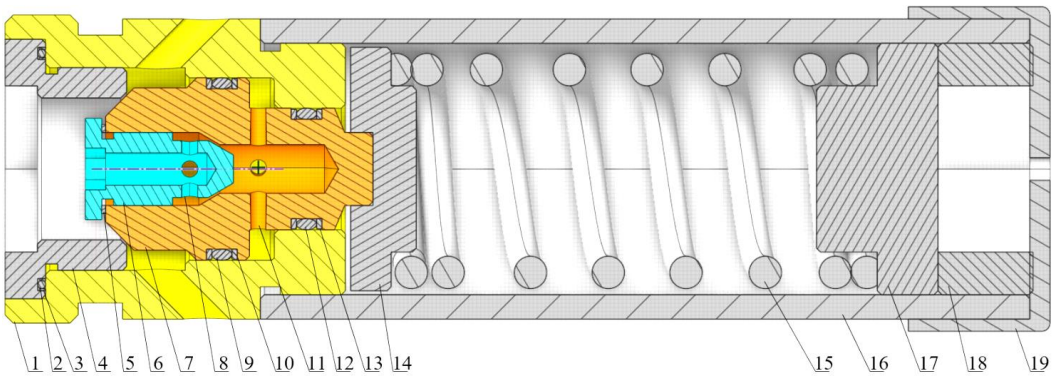

1. Valve sleeve 2, 9, 12. O-type seal ring 3, 10,13. Sealing ring retaining ring 4. Valve seat 5. Gasket 6. Damping conical throttle valve 7. Main valve core 8. Conical throttle valve damping hole 11. Main valve core damping hole 14. Spring seat 15. Spring 16. Sleeve 17. Spring adjustment seat 18. Spring thrust plug 19. Dust cover

Fig. 1 Differential large flow safety valve structure diagram

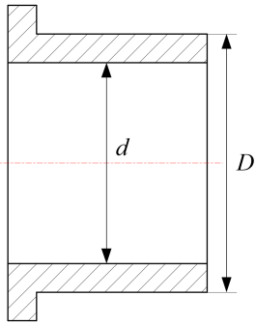

Fig. 2 Schematic diagram of valve seat structure

where, d is the diameter of the inlet, mm, Q_g is the rated flow of the differential large flow safety valve, L/min, V_g is the flow velocity of the valve seat inlet, m/s.

Since the liquid properties of high-water-based media bear a close resemblance to pure water, differential large-flow safety valves can be designed using pure water as the working medium. The internal flow pattern in these valves typically is typically turbulent. Consequently, for a given pressure loss, pure water requires a significantly higher flow rate than mineral hydraulic oil, leading to substantially increased fluid velocity. Theoretical calculations demonstrate that at equivalent cross-sectional areas, the permissible flow velocity for pure water is approximately 1.55 times that of mineral hydraulic oil. This fundamental principle allows for the modification of Eq. (1) as follows:

$$d \geq 0.372\sqrt{Q_g / V_g} \tag{2}$$

According to the actual working condition, V_g=35 m/s is selected and the inlet diameter d=35 mm is obtained after rounding.

According to the engineering experience, the wall thickness of the valve seat is set as 5mm, that is, the diameter of the valve seat D=35+5+5=45mm.

2.2 Main Valve Core Structure Design

To establish the connection between the main valve core and the differential chamber, a central bore is machined inside the core. The left end of this bore is threaded to secure the damping adjustment conical throttle valve, while the right end contains four damping holes. Due to the interference fit between the main valve core and the valve sleeve, the length of these damping holes cannot be modified. Therefore, damping regulation is achieved by adjusting the diameter of the damping holes.

The damping holes radius of the large flow safety valve used in mines is usually in the range of 1-3mm. Assuming that the damping holes radii of the main valve core are 1 mm, 2 mm and 3 mm respectively, the appropriate damping holes radius is selected according to the subsequent simulation results. The main valve core structure of the differential large flow safety valve is shown in Fig. 3.

According to the reference literature, the diameter of the safety valve core is D_1=(1.0~1.5)d. Therefore, the diameter of the main valve core is D_1=35 mm~52.5 mm, and D_1 is set to 42 mm.

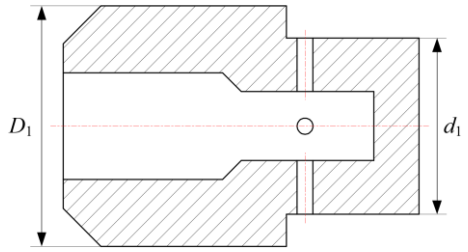

Fig. 3 Main valve core structure of differential large flow safety valve

The diameter of the main valve core is the same as that of the differential chamber. The cross-sectional area of the differential chamber is determined by the differential chamber diameter D_1 and the differential chamber small diameter d_1. Considering the working performance requirements of the differential large flow safety valve and the valve body size, the smaller diameter of the differential chamber d_1 is set to 33 mm.

In the unloading process of the differential large flow safety valve, the main valve core and the differential chamber are in relative motion. Therefore, the flow relationship between the damping hole and the differential chamber continuously evolving, as illustrated in Fig. 4.

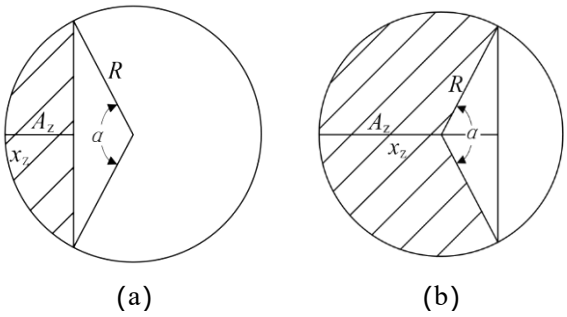

Fig. 4 Schematic diagram of damper hole fitting relationship

The calculation formula of the flow area of damping hole is as follows:

$$\begin{cases} A_z = 8\left[S_z - (R - x_z)\sqrt{2Rx_z - x^2}\right] & x_z \leq R \\ A_z = 8\left[\pi R^2 - S_z + (x_z - R)\sqrt{R^2 - (x_z - R)^2}\right] & x_z > R \end{cases} \tag{3}$$

Where, S_z is the bonding area between the damping hole and the differential cavity, mm^2, A_z is the flow area of the damping hole, mm^2, x_z is the axial overlapping distance between the damping hole and the differential cavity, mm, R is the radius of the damping hole, mm.

During the unloading process of the safety valve, if the displacement amplitude of the main valve core is too large, the internal pressure of the system will be out of control and operational safety will be reduced. Therefore, it is necessary to determine the maximum allowable displacement of the main valve core.

Displacement of the main valve core at maximum set pressure:

$$Q_g = C_d \pi D \sin\alpha_1 X_0 \sqrt{\frac{2g}{\gamma} p_{\max}} \tag{4}$$

This gives us:

$$X_0 = \frac{16.67 Q_g}{C_d \pi D \sin \alpha_1 \sqrt{\frac{2g}{\gamma} p_{\max}}} \tag{5}$$

Where, C_d is the flow coefficient, taken as 0.71, α_1 is the half-angle of the valve core cone angle, °, g is the gravitational acceleration, taken as 9.8 m/s^2, γ is the water's gravitational force, taken as 0.9737×10^-6 kgf/m, P_{max} is the maximum set pressure of the safety valve, taken as 50 MPa, X_0 is the maximum displacement of the main valve core, mm.

According to Eq. (5), the maximum displacement of the main valve core of the differential large flow safety valve is X_0=4.2 mm.

2.3 Valve Sleeve Structure Design

Owing to the structural constraints of differential large-flow safety valves, it is impossible to install multiple discharge ports on the main valve core. To achieve rapid unloading of the working medium, six evenly spaced discharge ports are arranged circumferentially are installed on the valve sleeve. When the differential large-flow safety valve operates at rated flow with stable unloading, the flow area of the discharge ports is given by the following formula:

$$A_1 = \frac{Q_g}{C_d \cdot \sin \alpha \cdot \sqrt{\frac{2}{\rho} \cdot P_0}} \tag{6}$$

where, A_1 is the flow area of the safety valve outlet, mm^2, ρ is the density of the working medium, 998kg/m3, P_0 is the pressure at the safety valve outlet, which is taken as 0.35MPa according to experience.

According to Eq. (6), we can get: $A_1 \approx 1068 \times 10^{-6}$m^2.

To facilitate the diffusion process during the unloading of the working medium and mitigate pressure impacts on the outlet wall, the valve sleeve's outlet is designed with six radially distributed cylindrical holes at 45° angles. As the unloading area must exceed the inlet area, calculations indicate that the outlet diameter should be set at 8 mm.

2.4 Structure Design of Damping Conical Throttle Valve

A damping-regulating conical throttle valve is installed in the central bore of the main valve core to meet diverse operational requirements and minimize the amplitude and frequency of valve core vibration during unloading. As shown in Fig. 5, this conical throttle valve has an M20×1.5 external thread and a 45° taper angle. Four damping holes of the same diameter are equally spaced along the axial direction of the valve body, matching the dimensions of the damping holes in the main valve core.

2.5 Spring Structure Design

The spring not only defines the operational performance requirements but also significantly affects the response sensitivity and dynamic characteristics of the safety valve. In this study, a cylindrical helical compression spring with a YI-type end structure was selected, the schematic of which is presented in Fig. 6.

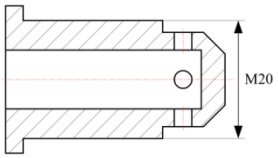

Fig. 5 Structure of damping regulating conical throttle valve

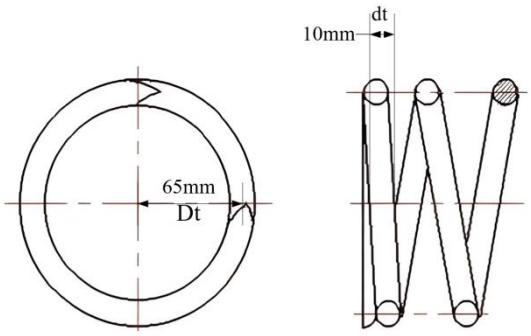

Fig. 6 Structure of cylindrical helical compression spring

The spring material is selected as 65Mn. The spring parameters of 65Mn material are: shear modulus G is 78500 MPa, tensile strength R_m is 1320 MPa, allowable shear stress τ is 660 MPa, spring wire diameter d_t is 10 mm, and spring middle diameter, and D_t is 65 mm.

The calculation formula of spring effective number of turns n_1 is:

$$n_1 = \frac{G d_t^4}{8 D_t^3 F_1} f_1 \tag{7}$$

where, F_1 is the working load of the spring, N. f_1 is the deformation under the working load of the spring, mm.

According to Eq. (7), the effective number of turns is 6, and the actual number of turns is 8 because the spring adopts Y_1 type end structure.

The calculation formula of spring twist ratio and curvature coefficient is as follows:

$$C = \frac{D_t}{d_t} \tag{8}$$

$$K_1 = \frac{4C-1}{4C-4} + \frac{0.615}{C} \tag{9}$$

where, C is the spring winding ratio, K_1 is the spring curvature coefficient.

According to Eq. (8) and Eq. (9), C=6.5 and K_1=1.23 can be obtained by substituting each parameter.

The calculation of some important parameters of spring part is as follows:

$$t = d_t + \frac{f_1}{n_1} \tag{10}$$

$$H_0 = n_1 t + 1.5 d_t \tag{11}$$

$$a_t = \arctan \frac{t}{\pi D_t} \tag{12}$$

$$L = \frac{\pi D_t n_1}{\cos a} \approx \pi D n_1 \tag{13}$$

where, t is the spring pitch, H_0 is the free height of the spring, at is the spring helix Angle, L is the spring extension length.

According to Eq. (10)-Eq. (13), after rounding all parameters, we can get: t=26 mm, H_0=171 mm, a_t=7°, and L=1131 mm.

3. DYNAMIC CHARACTERISTICS OF FLUID WITH DIFFERENT DAMPING HOLE RADIUS IN DIFFERENTIAL LARGE FLOW SAFETY VALVE

To determine the optimal radius of the damping holes in a differential high-flow safety valve design, we conducted simulations using Fluent's dynamic mesh technology and User-Defined Functions (UDF) for fluid transient characteristics during the valve's operation from opening to stable unloading (Liu et al., 2025). Through comprehensive evaluation of transient performance and operational stability analysis results, the optimal damping holes radius was identified.

3.1 Flow Channel Model and Grid Division

To maintain computational accuracy, the flow channel geometry was simplified by removing minor features such as guide vanes, fillets, and threads. The deformation zones were uniformly defined as deforming, and the interface between the damping holes and differential chambers was designated as interface. The moving regions were labeled as moving, while the inlet and outlet ports were set as inlet and outlet respectively. All other surfaces were uniformly defined as walls. The geometric model of the differential high-flow safety valve flow channel is shown in Fig. 7.

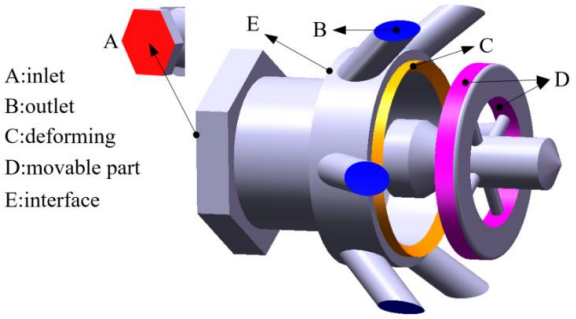

Fig. 7 Geometric model of flow channel of differential large flow safety valve

The Fluent meshing module is used to divide the flow channel geometric model of the differential large flow safety valve into a grid. Set the mesh type to tetrahedral, locally encrypted, orthogonal quality 0.88 , skewness 0.62, aspect ratio 1.84. The flow channel grid model of the differential large flow safety valve is shown in Fig.8.

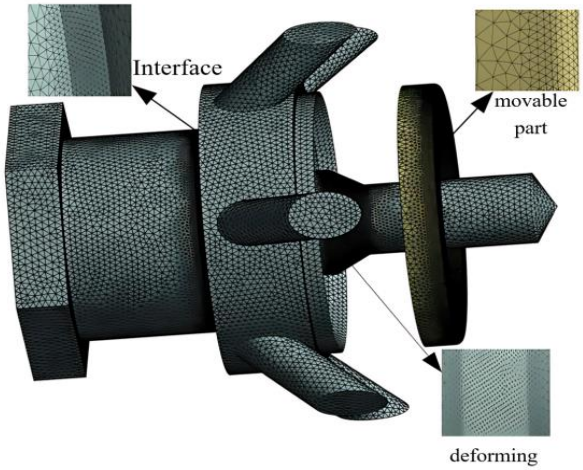

Fig. 8 Flow channel mesh model

3.2 SETTING OF BOUNDARY CONDITIONS

Through the UDF compilation function of Fluent platform, the coupled motion between the main valve core and fluid is described. The surface of the main valve core is set as a sliding wall, while other parts are non-sliding walls. The working medium is set as pure water, and the internal fluid in the safety valve is incompressible. The relevant boundary conditions are shown in Table 1.

In this paper, the SIMPLE algorithm based on the velocity-pressure coupling correction is used to discretise the computational model. The discretised momentum equation for the SIMPLE algorithm is:

$$\begin{cases} a_{i,j}u^*_{i,j} = \sum a_{nb}u^*_{nb} + (u^*_{i-1,j} - u^*_{i,j}) + u^*_{i,j} \\ a_{i,j}v^*_{i,j} = \sum a_{nb}v^*_{nb} + (v^*_{i,j-1} - v^*_{i,j}) + v^*_{i,j} \end{cases} \tag{14}$$

Where: a,$b$is the coefficient term and the constant term; the u,v is the initial value of the velocity component, and the others are terms related to the number of iterations. When the initial iteration is performed, define the initial value of pressure p^*, According to Eq. (14), the velocity components u^*,v^* can be determined after the first iteration. The initial pressure value p^* is then adjusted based on these velocity components. The pressure correction equation is:

$$\begin{aligned} a_{i,j}p'_{I,J} = {} & a_{I,J}p'_{J-1,I} + a_{I-1,J}p'_{J-1,I} + \\ & a_{I,J-1}p'_{J,I+1} + a_{I,J-1}p'_{J,I+1} + b'_{I,J} \end{aligned} \tag{15}$$

Table 1 Key boundary conditions Settings

order number	bounds	Definition of boundary conditions for computational domains	numeric value
1	Surface of inlet port	Pressure-inlet	50MPa
2	Surface of the outlet	Pressure-outlet	0MPa
3	Fluid wall	Wall	——

The velocity values are corrected using the corrected pressure values p' and velocity components u*,v* and the velocity correction equation is:

$$\begin{cases} p'_{I,J} = p_{I,J} + p'_{I,J} \\ u_{i,j} = u^*_{i,J} + \dfrac{A_{i,J}}{a_{i,J}}(p'_{I+1,J} - p'_{I,J}) \\ v_{i,j} = v'_{I,j} + \dfrac{A_{I,j}}{a_{I,j}}(p'_{I,j-1} - p'_{I,J}) \end{cases} \tag{16}$$

where : A is the area of the computational microelement. The turbulent transport equation has to be introduced in the turbulence model calculations. The turbulence transport equation for the simulation is:

$$\begin{cases} \dfrac{\partial(\rho k)}{\partial t} + \dfrac{\partial(\rho k u_i)}{\partial x_i} = \dfrac{\partial}{\partial}\left(\alpha_k u_{eff}\dfrac{\partial k}{\partial x_j}\right) + G_k - \rho\varepsilon \\ \dfrac{\partial}{\partial t}(\rho\varepsilon) + \dfrac{\partial}{\partial x_i}(\rho\varepsilon u_i) = \dfrac{\partial}{\partial x_j}\left(\alpha_\varepsilon u_{eff}\dfrac{\partial \varepsilon}{\partial x_j}\right) + \\ \qquad C_{1\varepsilon}\dfrac{\mathrm{G}_k\,\varepsilon}{k} - \mathrm{C}_{2\varepsilon}\dfrac{\rho\varepsilon^2}{k} \end{cases} \tag{17}$$

where: ρ is the density of the fluid; ueff is the turbulent viscosity; k is the turbulent energy; ε is the turbulent dissipation rate; $C_{1\varepsilon}$, $C_{2\varepsilon}$, a_ε, a_ε are the turbulence model constants.

The coefficient terms in the discrete equations are solved based on the turbulent flow, and the equations are calculated as:

$$\begin{aligned} a_{I,J}\phi_{I,J} = {} & a_{I-1,J}\phi_{I+1,J} - a_{I-1,J}\phi_{I-1,J} + \\ & a_{I,J-1}\phi_{I,J-1} + a_{I,J-1}\phi_{I,J-1} + b'_{I,J} \end{aligned} \tag{18}$$

where: Φ is the diffusion term generic variable.

This study adopts the RNG k-ε turbulence model by incorporating an additional term into its turbulence dissipation rate equation. Compared with standard models, this approach accounts for the influence of vortices on fluid dynamics in turbulent states, thereby improving computational accuracy for vortex regions within flow channels. By applying statistical methods from renormalization group theory, the viscosity of fluids remains unaffected by variations in their physical parameters. This enables effective treatment of low-Reynolds-number flows within near-wall boundary layers. Consequently, the RNG k-ε turbulence model has been selected as the preferred choice in this research.

The motion law of the main valve core was defined by the pre-compiled macro DEFINE_CG_MOTION of Fluent UDF, and the method of combining mesh smoothing and mesh reconstruction was adopted to update the mesh in the moving area. The equation can be expressed as:

$$\begin{aligned} \frac{\mathrm{d}}{\mathrm{d}t}\int_V \rho\phi \mathrm{d}V + \int_{\partial V}\rho\phi\left(u - u_{\mathrm{g}}\right)\cdot \mathrm{d}A = {} & \int_{\partial V}\Gamma\nabla\phi\cdot\mathrm{d}A + \\ & \int_V S_\phi \mathrm{d}V \end{aligned} \tag{19}$$

where: s_Φ is the source term; is the boundary of the control volume microelement; u_g is the velocity vector of the moving mesh; Γ is the fluid diffusion coefficient; and A is the moving mesh cross-sectional area.

The simulation time is set to 0.03 s and the time step size is set to 1e-5s, so as to simulate the transient characteristics of the fluid during the process from opening to stable unloading of the safety valve.

A standard initialisation scheme was used in Fluent, compute from Inlet, Reference frame set as relative to cell zone, gauge pressure is 0.1 MPa, turbulence intensity value of 5%, and convergence criteria residuals of 1e-4. In order to ascertain that the number of model grids and their sizes were approximately independent of numerical simulations, a grid independence test was carried out. approximately independent of the numerical simulation results, a grid independence test was carried out.

Given that the safety valve flow path model contains multiple interconnected fluid domains and each subdomain has a differentiated grid size, the mobile region with significant flow characteristics is selected as the object of grid irrelevance verification in this study. The flow monitoring data of the six outlets of the safety valve are used as the discriminative index of grid irrelevance, and the grid division is shown in Table 2, and the results of grid irrelevance validation are shown in Fig. 9.

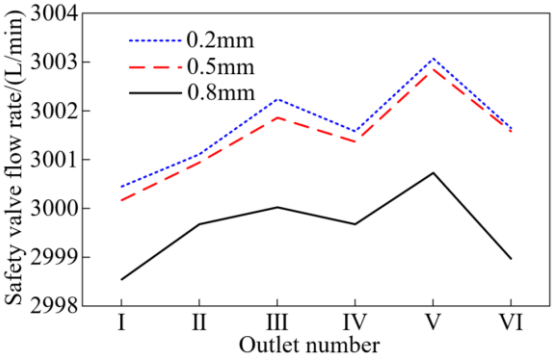

Fig. 9 Grid independence results

Table 2 Grid division situations in different sizes

Grid size/mm	Number of grid cells	Grid quality
0.2	10425	0.932
0.5	4873	0.928
0.8	2557	0.905

As shown in Fig. 9 the size of the outlet flow rate is virtually identical when the grid size is 0.2 mm and 0.5 mm, indicating that the increase in the number of grids has a very small effect on the outlet flow rate. Therefore, choosing the grid size of 0.5 mm for subsequent simulation can effectively improve the simulation efficiency and reduce the time cost.

3.3 EXPERIMENTAL VERIFICATION

In order to verify the feasibility of the numerical simulation work, experimental tests were carried out on the safety valve samples under the same conditions, and the comparative results of the simulation tests obtained are shown in Fig. 10.

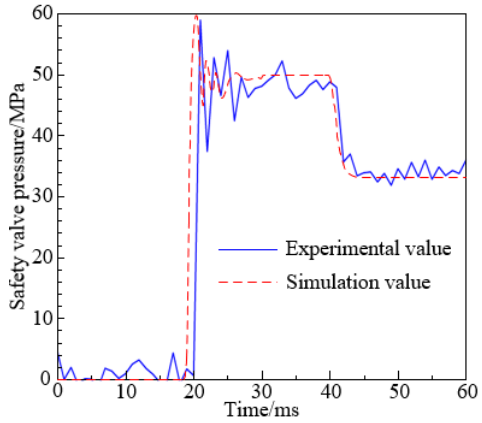

(a) pressure

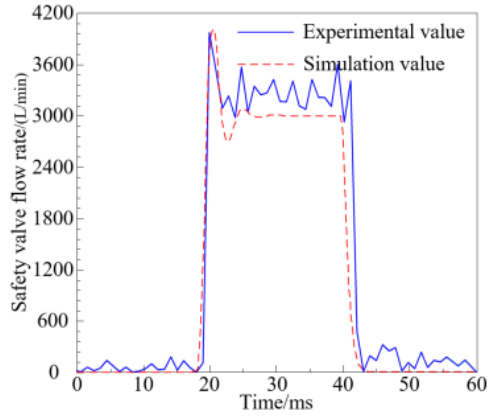

(b) flow rate

Fig. 10 Comparison results of simulation experiments

As can be seen from Fig. 10, the simulation result of the peak pressure of the safety valve is 59.8 MPa, and the test result is 58.6 MPa, and the simulation result of the steady state pressure of the safety valve is 48.1 MPa, and the test result is 46.2 MPa, with an average error of 4.6%.

The simulation result of the peak flow rate of the safety valve is 3955 L/min, and the test result is 3842 L/min, and the simulation result of the steady flow rate of the safety valve is 2986 L/min, and the test result is 3098L/min, with an average error of 4.2%. Therefore, the results of numerical simulation can reflect the actual situation to a certain extent, and the established simulation model can be used to carry out the next study.

3.4 Analysis of Transient Characteristics of Fluid with Different Damping Hole Radii

The simulation results of five important moments were selected for comparative analysis, which are: the moment of safety valve opening (t=0.1 ms), the moment when the valve core displacement reaches small opening degree (t=0.6 ms), the moment when the valve core displacement reaches medium opening degree (t=1.2 ms), the moment when the valve core displacement reaches maximum opening degree (t=2.2 ms) and the moment when the safety valve is stable unloading (t=20 ms).

3.4.1 Analysis of Transient Characteristics of Fluid with Damping Hole Radius of 1mm

When time t=0.1 ms, 0.6 ms, 1.2 ms, 2.2 ms and 20 ms, the pressure and velocity distribution results of the internal flow field of the differential large flow safety valve are shown in Fig. 11 to Fig. 15 respectively.

As shown in Fig. 11, the fluid velocity in the flow path between the inlet and outlet ports reaches a peak velocity of 356.1 m/s. The damping effect of the conical throttle valve and damping holes causes the velocity within the main valve core's central hole to be lower than that in the inlet region. The instantaneous opening of the safety valve core triggers structural changes in the flow path between the ports, converting the fluid's pressure potential energy into kinetic energy. This leads to an

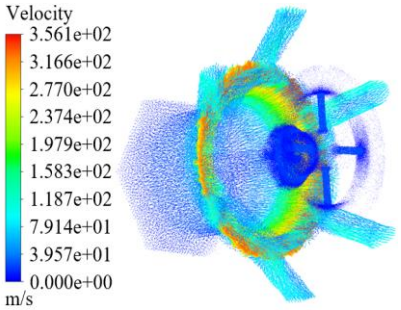

(a) Three-dimensional velocity vector diagram

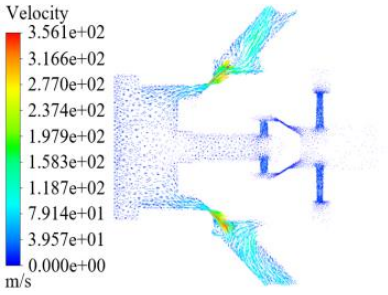

(b) Velocity vector diagram of XY section

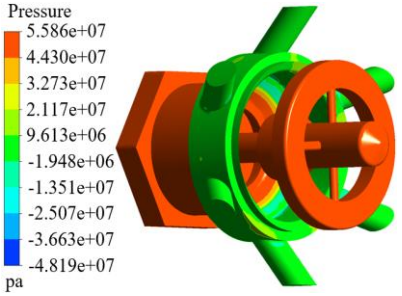

(c) 3d pressure cloud

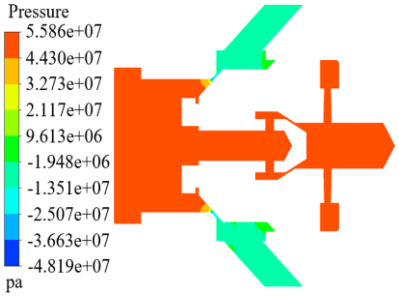

(d) XY section pressure cloud diagram

Fig. 11 t=0.1 ms Flow field velocity and pressure distribution

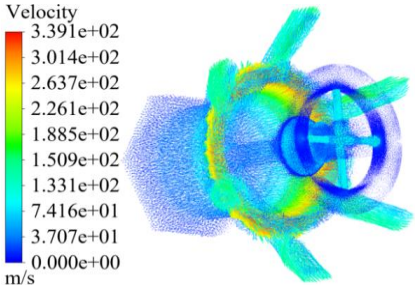

(a) 3d velocity vector diagram

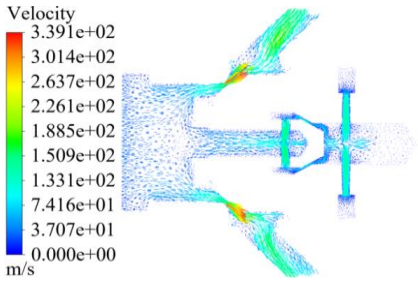

(b) Velocity vector diagram of XY section

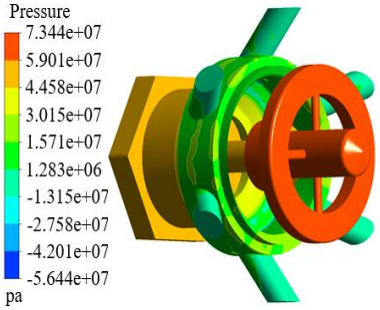

(c) 3d pressure cloud

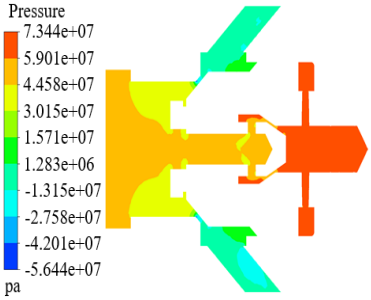

(d) XY section pressure cloud

Fig. 12 *t*=0.6 ms Flow field velocity and pressure distribution

increased pressure gradient, elevating the flow field's peak pressure to 55.86 MPa. Localized negative pressure zones emerge in the flow field, mirroring the distribution of high-velocity regions-a phenomenon consistent with Bernoulli's principle. The intense velocity shear effects in the high-speed areas induce cavitation and backflow phenomena near the outlet port.

As shown in Fig. 12, compared to the t=0.1 ms state, the valve core displacement gradually increases, resulting in a corresponding expansion of the flow area between the inlet and outlet ports. This leads to a reduction in peak flow velocity to 339.1 m/s, while both the outlet region and the interior of the main valve core's central bore experience increased flow velocities. Due to the strong damping effect from the conical throttle valve and damping holes at this stage, fluid motion must overcome greater resistance, triggering the conversion of fluid pressure potential energy into internal energy. This energy conversion mechanism elevates the flow field pressure peak to 73.44 MPa, with high-pressure regions concentrated at the right end of the central bore and the differential chamber area. The expanded flow area exacerbates discontinuity in velocity gradient distribution, thereby expanding the negative pressure zones within the flow field.

As shown in Fig. 13, compared to the t=0.6 ms state, the valve core displacement gradually increases. The flow area between the inlet and outlet expands, causing the peak flow velocity to decrease to 310.1 m/s while the velocity in the outlet region rises. With reduced inflow into the central orifice of the main valve core, the damping effect of the conical throttle valve and damping holes diminishes. The peak pressure in the flow field decreases to 67.09 MPa, with the distribution of high-pressure and low-pressure zones remaining largely unchanged. However, the low-pressure region near the wall at the outlet's corner expands significantly.

As shown in Fig. 14, when t=2.2 ms is applied, the valve core displaces to its maximum opening position. The flow area between the inlet and outlet reaches its peak, with the velocity peak decreasing to 298.8 m/s while the outlet region achieves maximum velocity. At this stage, the conical throttle valve and damping holes become nearly ineffective, reducing the pressure peak in the flow field to 55.34 MPa. The internal pressure gradient distribution within the flow channel remains relatively uniform, with negative pressure zones concentrated only near the wall at the outlet's corner. These negative pressure areas show relative reduction in intensity.

As shown in Fig. 15, compared to the t=2.2 ms state, the valve core displacement decreases, resulting in reduced flow area between the inlet and outlet ports. The peak flow velocity increases to 324.5 m/s, while the velocity in the outlet region decreases. The pressure distribution across the flow field becomes more uniform, with the negative pressure zone remaining largely unchanged but showing a reduction in its size. The pressure gradient near the wall surface also diminishes. Both the central orifice of the main valve core and the inlet region maintain nearly identical pressure values at 50 MPa, with stable trends observed in both flow velocity and pressure fluctuations.

In summary, as the t=0.1 ms value increases to t=2.2 ms, the differential displacement of the large-flow safety valve core grows proportionally. This expansion enlarges the flow area between the inlet and outlet ports, resulting in reduced peak flow velocity while increasing downstream velocity at the outlet. The damping effects of conical throttle valves and orifice plates directly influence the maximum pressure in the flow field. When t=0.6 ms,

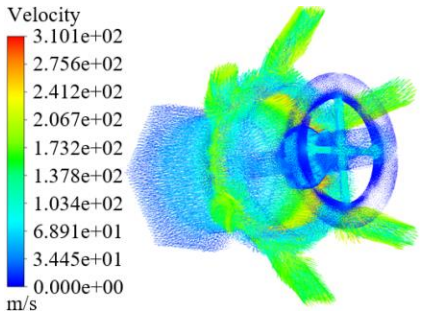

(a) 3d velocity vector diagram

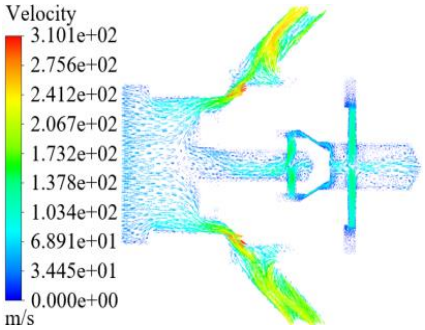

(b) Velocity vector diagram of XY section

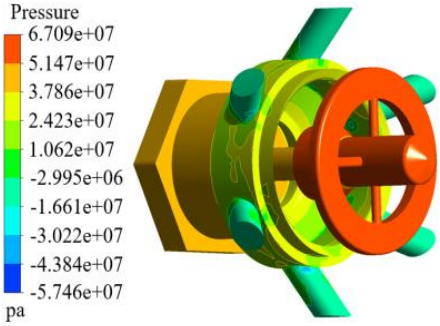

(c) 3d pressure cloud

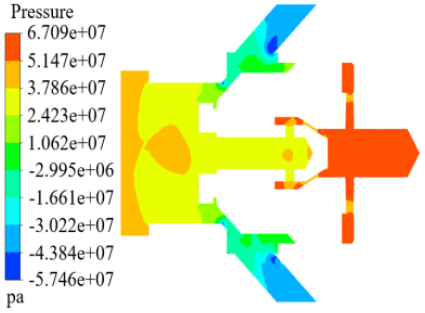

(d) XY section pressure cloud

Fig. 13 *t*=1.2 ms Flow field velocity and pressure distribution

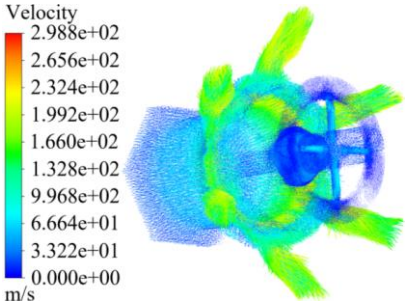

(a) Three-dimensional velocity vector diagram

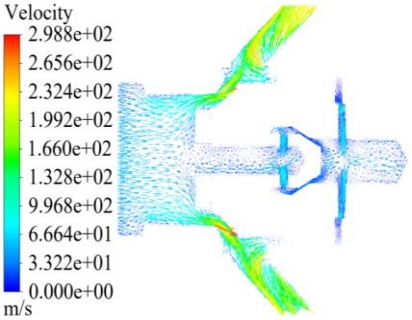

(b) Velocity vector diagram of XY section

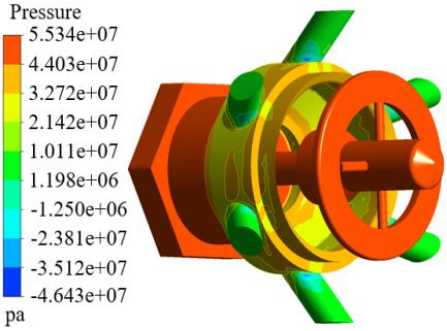

(c) 3d pressure cloud

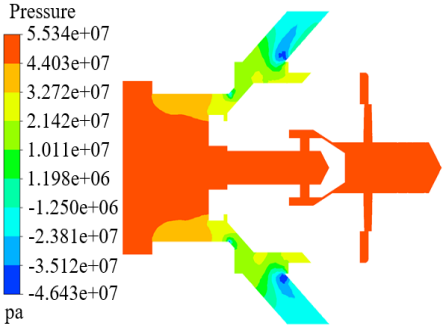

(d) XY section pressure cloud

Fig. 14 *t*=2.2 ms Flow field velocity and pressure distribution

the damping effect becomes most pronounced, causing the peak pressure to rise to 73.44 MPa. This significantly compromises the operational stability of the safety valve and heightens the potential risk of operational failure.

The negative pressure region in the flow field expands, making it highly susceptible to cavitation and backflow phenomena. These issues severely compromise the safety valve's operational stability and service life. When t=20 ms, the safety valve achieves stable unloading. The conical throttle valve and damping holes fail to function as intended. This necessitates comparative analysis of the fluid transient characteristics during the process where t=0.1 ms increases to t=2.2 ms.

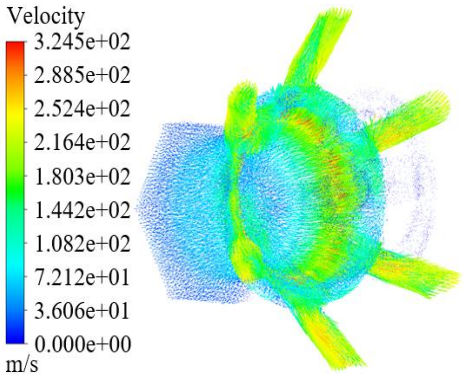

(a) Three-dimensional velocity vector diagram

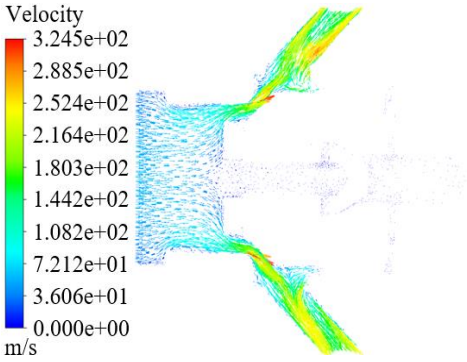

(b) Velocity vector diagram of XY section

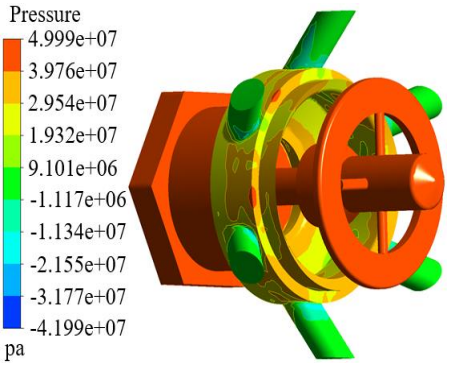

(c) 3d pressure cloud

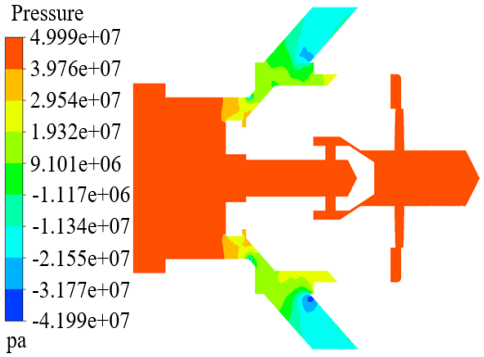

(d) XY section pressure cloud

Fig. 15 shows the velocity and pressure distribution of the flow field at *t*=20 ms

Therefore, when the damping hole radius of the differential large flow safety valve is 1mm, the pressure peak in the flow field is large during unloading, which seriously affects the working stability of the safety valve.

3.4.2 Analysis of Transient Characteristics of Fluid with Damping Hole Radius of 2mm

When time t=0.1 ms, 0.6 ms, 1.2 ms and 2.2 ms, the pressure and velocity distribution results of the internal flow field of the differential large flow safety valve are shown in Fig. 14 to Fig. 17 respectively.

As shown in Fig. 16, the safety valve's internal flow field exhibits velocity peaks of 363.7 m/s and pressure peaks of 54.66 MPa. Compared to the scenario with a damping holes radius of 1mm at the same moment, the flow velocity distribution pattern shows nearly identical characteristics. The velocity peak is relatively higher while the pressure peak decreases, resulting in reduced pressure gradient between the inlet and outlet ports and enhanced fluid flow stability.

As shown in Fig. 17, the safety valve's internal flow field exhibits a peak velocity of 343.0 m/s and a peak pressure of 64.08 MPa. Compared to the scenario with a damping holes radius of 1mm at the same moment, the velocity peak has increased while the pressure peak has decreased. The enhanced damping effect from the larger orifice radius results in reduced damping effects on both the conical throttle valve and the orifice itself. Consequently, the velocity fluctuations within the main valve core's central orifice become more controlled, leading to a more uniform pressure distribution. Although the negative pressure zones maintain similar spatial patterns, their reduced magnitude significantly lowers the likelihood of cavitation and backflow phenomena within the valve's internal fluid flow.

As shown in Fig. 18, the safety valve's internal flow field exhibits a peak velocity of 311.0 m/s and a pressure peak of 60.26 MPa. Compared to the scenario with a damping holes radius of 1mm at the same moment, the velocity peak shows relative improvement. The velocity variation within the main valve core's central orifice remains relatively small, while the outlet region demonstrates increased velocity. Conversely, the pressure peak decreases, resulting in more uniform pressure distribution, reduced negative pressure zones, and diminished pressure gradients near the outlet wall. These modifications effectively minimize fluid separation from the wall and subsequent vortex formation.

As shown in Fig. 19, the safety valve's internal flow field exhibits a peak velocity of 300.5 m/s and a peak pressure of 53.97 MPa. Compared to the scenario with a damping holes radius of 1mm at the same moment, the velocity peak has increased relatively. The velocity variation within the main valve core's central orifice remains relatively small, while the outlet area shows enhanced velocity. Conversely, the pressure peak decreases proportionally, resulting in more uniform pressure distribution across the outlet region. These improvements help reduce vibration and noise generated during the safety valve's unloading process.

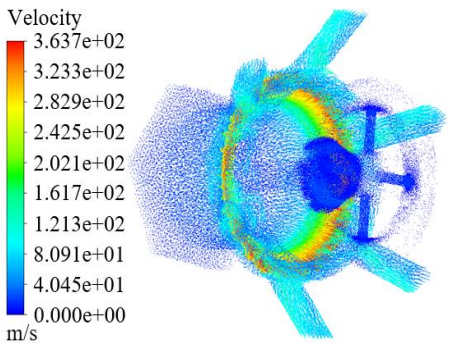

(a) Three-dimensional velocity vector diagram

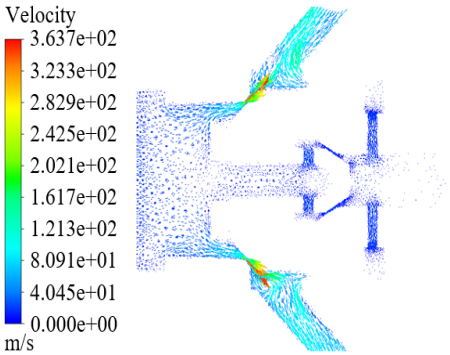

(b) Velocity vector diagram of XY section

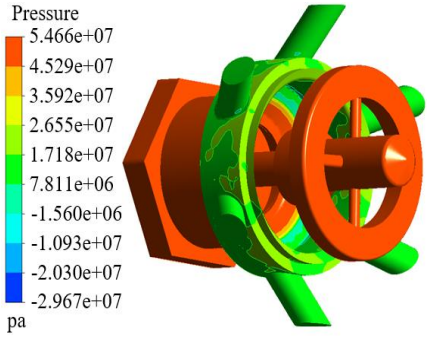

(c) 3d pressure cloud

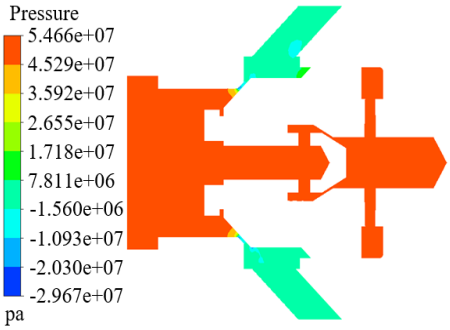

(d) XY section pressure cloud

Fig. 16 *t*=0.1 ms Flow field velocity and pressure distribution

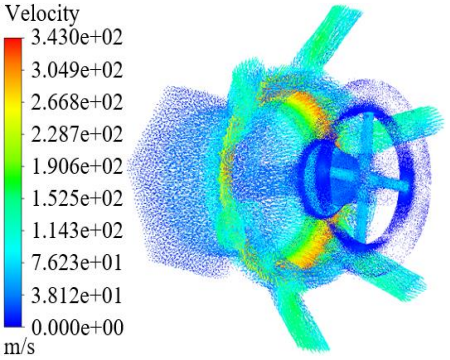

(a) 3d velocity vector diagram

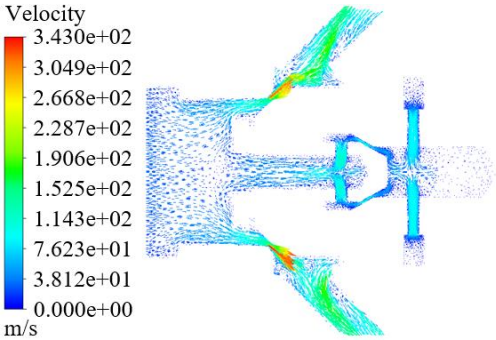

(b) Velocity vector diagram of XY section

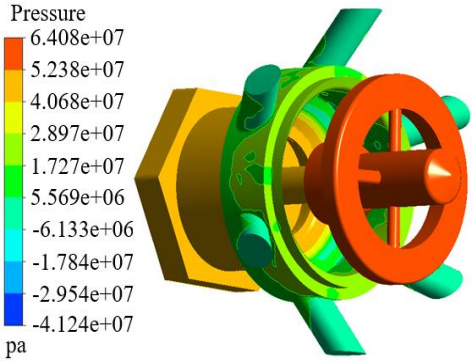

(c) 3d pressure cloud

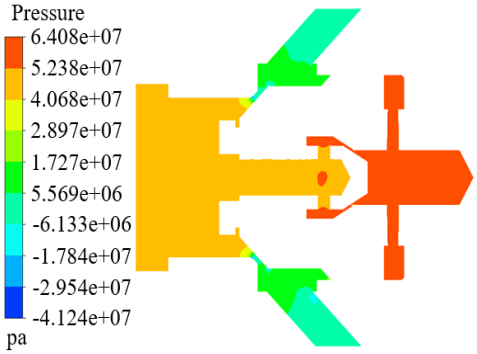

(d) XY section pressure cloud diagram

Fig. 17 *t*=0.6 ms Flow field velocity and pressure distribution

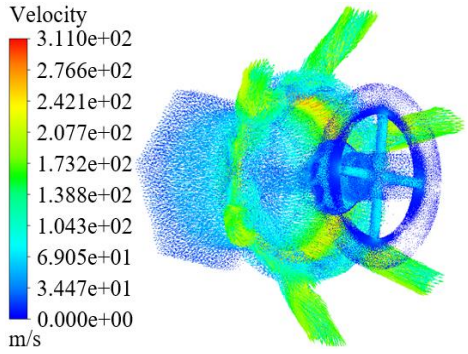

(a) Three-dimensional velocity vector diagram

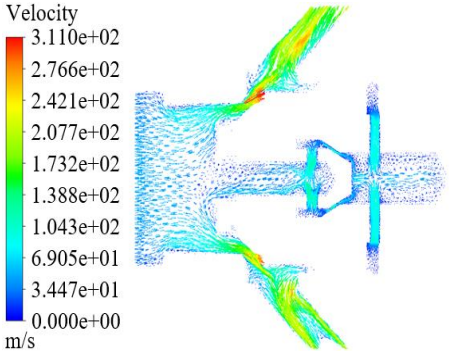

(b) Velocity vector diagram of XY section

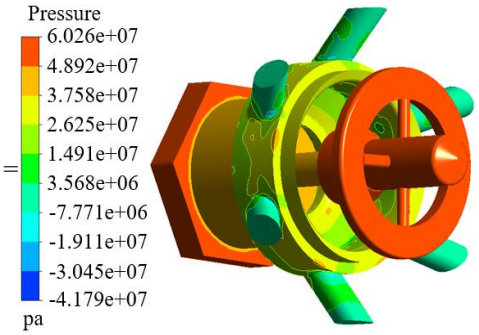

(c) 3d pressure cloud

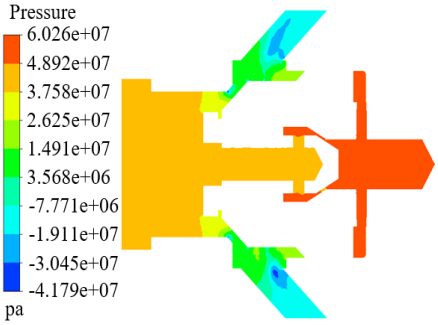

(d) XY section pressure cloud

Fig. 18 *t*=1.2 ms Flow field velocity and pressure distribution

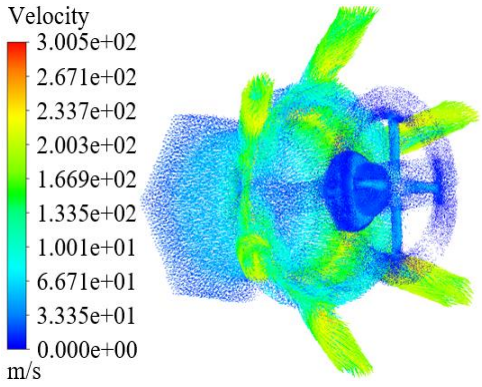

(a) Three-dimensional velocity vector diagram

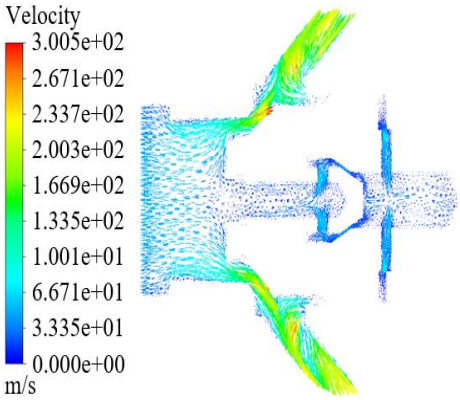

(b) Velocity vector diagram of XY section

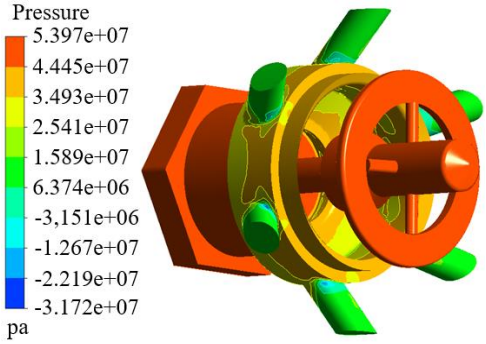

(c) 3d pressure cloud

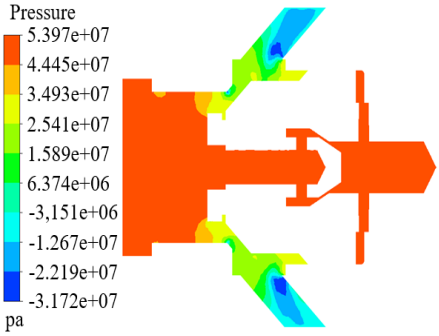

(d) XY section pressure cloud

Fig. 19 *t*=2.2 ms Flow field velocity and pressure distribution

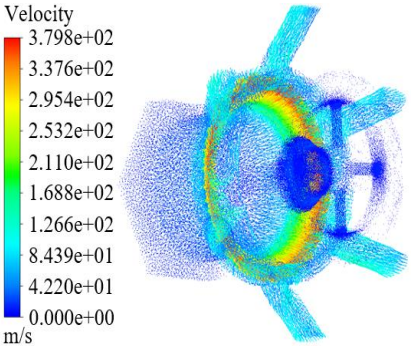

(a) 3d velocity vector diagram

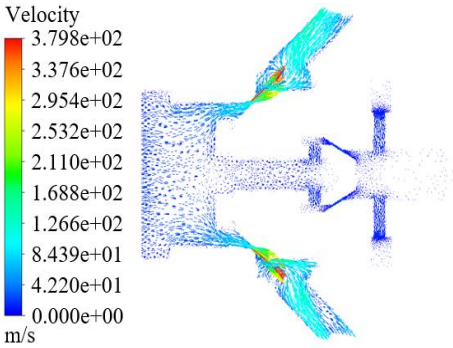

(b) Velocity vector diagram of XY section

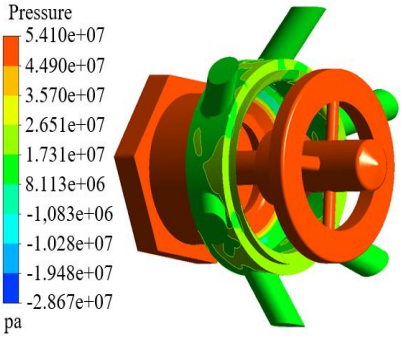

(c) 3d pressure cloud

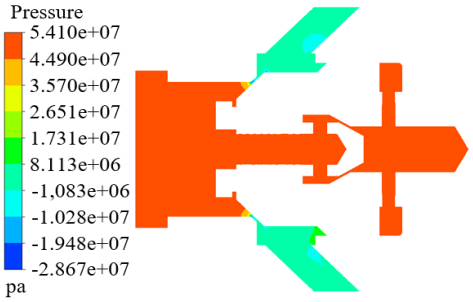

(d) XY section pressure cloud

Fig. 20 *t*=0.1 ms Flow field velocity and pressure distribution

3.4.3 Analysis of Transient Characteristics of Fluid with Damping Hole Radius of 3 mm

When time *t*=0.1 ms, 0.6 ms, 1.2 ms and 2.2 ms, the pressure and velocity distribution results of the internal flow field of the differential large flow safety valve are shown in Fig. 20 to Fig. 23 respectively.

As shown in Fig. 20, the safety valve's internal flow field exhibits a peak velocity of 379.8 m/s and a peak pressure of 54.10 MPa. Compared with the results obtained when the damping holes radius was 1 mm and 2 mm at the same moment, this configuration demonstrates the highest relative velocity peak, the lowest relative pressure peak, the smallest pressure gradient in the fluid passage between the inlet and outlet, and the best fluid flow stability.

As shown in Fig. 21, the safety valve exhibits a flow velocity peak of 349.2 m/s and a pressure peak of 59.79 MPa within its internal flow field. Compared to the results obtained with damping holes of 1 mm and 2 mm at the same moment, this configuration demonstrates the highest relative velocity peak, the smallest variation in fluid velocity within the main valve core's central orifice, and the lowest relative pressure peak. However, when compared to the case with a 2 mm damping holes, the pressure gradient distribution in the inlet area becomes uneven, resulting in relatively lower operational stability of the safety valve.

As shown in Fig. 22, the safety valve's internal flow field exhibits a peak velocity of 313.9 m/s and a pressure peak of 56.03 MPa. Compared to the results with damping holes of 1 mm and 2 mm at the same moment, this configuration demonstrates the highest relative velocity peak, the smallest variation in fluid velocity within the main valve core's central orifice, the maximum velocity in the outlet region, and the lowest pressure peak. However, when compared to the 2 mm damping hole configuration, the pressure gradient near the wall at the outlet becomes significantly larger, increasing the probability of vortex formation caused by fluid separation from the wall surface.

As shown in Fig. 23, the safety valve's internal flow field exhibits peak velocity of 308.2 m/s and pressure of 51.03 MPa. Compared with the results obtained at the same moment using damping holes with radii of 1mm and 2mm, this configuration demonstrates the highest velocity peak, maximum flow rate in the outlet region, lowest pressure peak, and minimal negative pressure area. The velocity and pressure distribution patterns are nearly identical to those observed when using damping holes with a 2 mm radius.

A comprehensive comparison of safety valves with damping hole radii of 1 mm, 2 mm, and 3 mm, it is evident that their flow velocity patterns and pressure distribution characteristics during the initial opening phase (*t*=0.1 ms) are nearly identical. The valve with a 1mm orifice exhibits the most significant velocity fluctuations, demonstrates the most complex pressure distribution, and achieves the highest pressure peak. This indicates that the 1 mm orifice performs the least stable under unloading conditions, posing the greatest risk of cavitation and backflow phenomena. In contrast, the 3 mm orifice shows minimal variation in internal velocity, maximum flow velocity in the outlet region, and the lowest pressure peak. Due to its relatively larger orifice size, when the valve core displaces to moderate opening degrees, the conical throttle valve and damping hole lose effectiveness. Compared to the 2 mm orifice, the 3 mm valve displays a more pronounced and uneven pressure gradient near the wall surface,

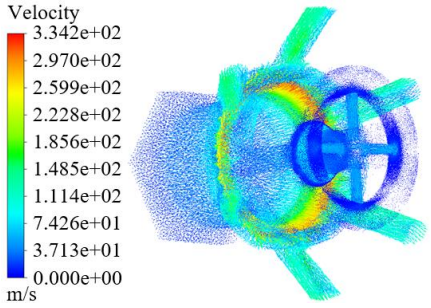

(a) 3d velocity vector diagram

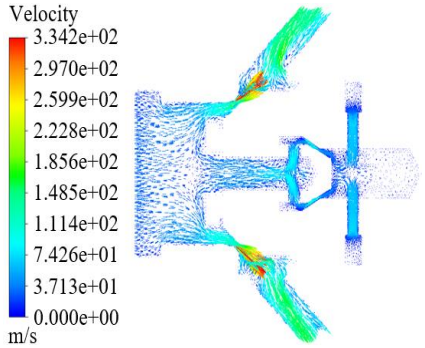

(b) Velocity vector diagram of XY section

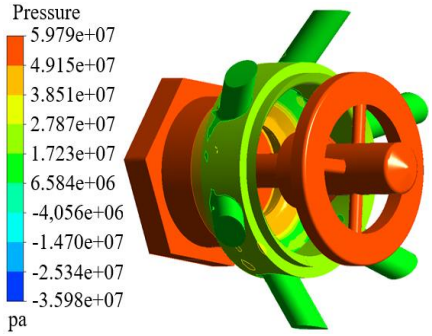

(c) 3d pressure cloud

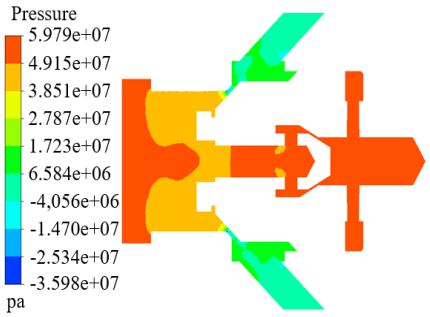

(d) XY section pressure cloud

Fig. 21 *t*=0.6 ms Flow field velocity and pressure distribution

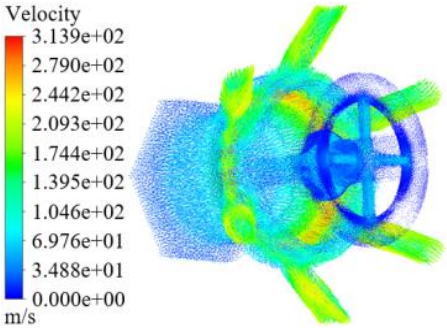

(a) Three-dimensional velocity vector diagram

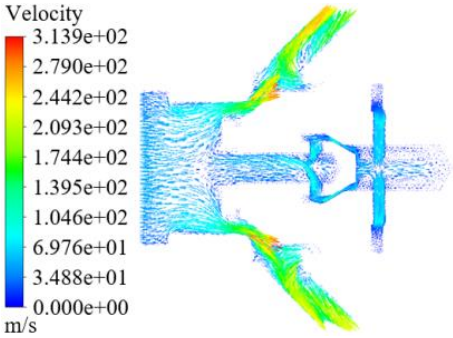

(b) Velocity vector diagram of XY section

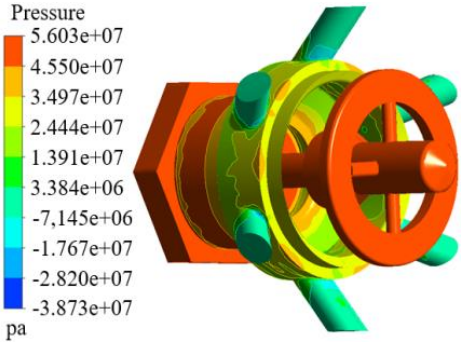

(c) 3d pressure cloud

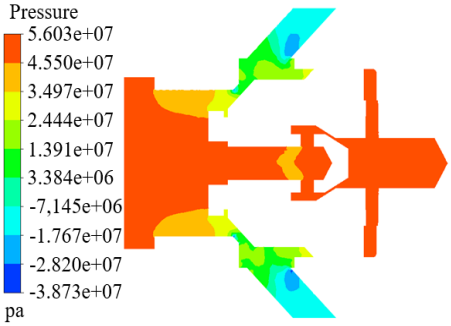

(d) XY section pressure cloud

Fig. 22 *t*=1.2 ms Flow field velocity and pressure distribution

increasing the likelihood of fluid separation from the wall and vortex formation. The 2 mm orifice maintains balanced pressure and velocity variations with higher flow stability, avoiding excessive pressure spikes. During unloading processes, it effectively provides damping while ensuring operational stability.

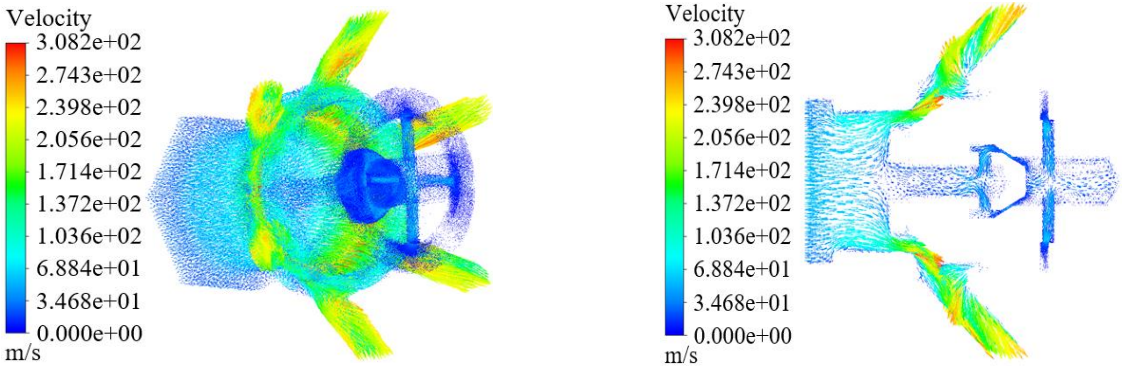

(a) Three-dimensional velocity vector diagram

(b) Velocity vector diagram of XY section

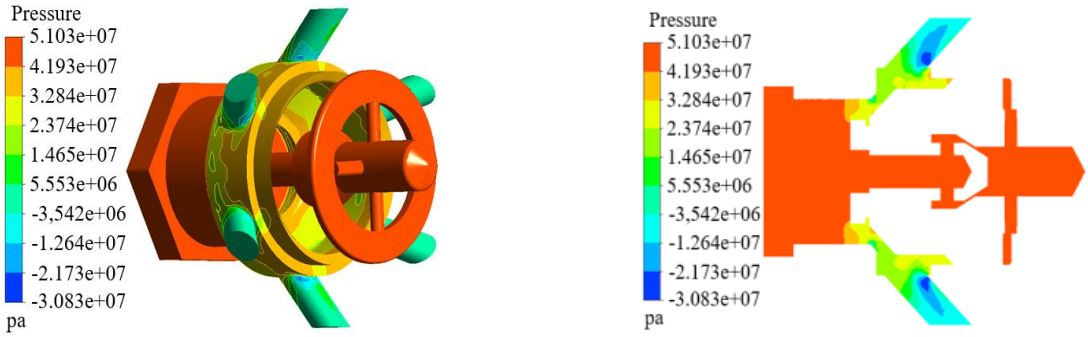

(c) 3d pressure cloud

(d) XY section pressure cloud

Fig. 23 *t*=2.2 ms Flow field velocity and pressure distribution

In order to more clearly compare the effect of damping hole size on the fluid flow characteristics of differential high flow safety valves, the fluid pressure characteristics were selected as the main comparative parameter, Fig. 24 shows the peak pressure change curve of the fluid during the process of assembling different sizes of damping holes in the differential high flow safety valves from the opening to the spool displacement to the maximum opening degree.

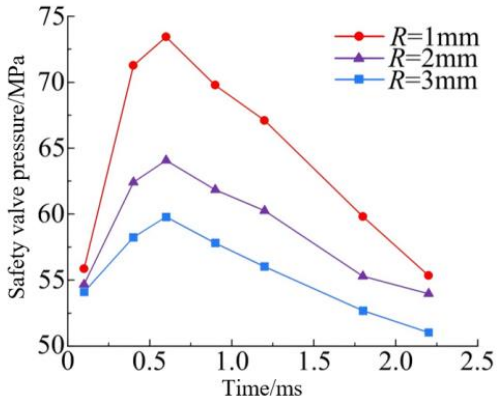

Fig. 24 Peak pressure

As can be seen from the figure, the peak pressure and the pressure change of the fluid inside the flow path of the differential high flow safety valve with *R*=1mm damping hole is the largest. This is because the smaller size of the damping hole plays a larger damping effect on the fluid, resulting in the fluid flow through the centre hole of the main spool, it will be subject to a greater resistance resulting in a rapid reduction in the flow rate, but the inlet of high-pressure fluid is still flowing into the inlet, resulting in a rapid increase in the pressure of the fluid inside the centre hole. Even when the spool is displaced to a small opening position, the pressure overshoot of the safety valve far exceeds the national standard. Although the differential high flow safety valve assembled with *R*=3 mm damping holes has the smallest pressure peak and pressure change inside the flow path, the damping effect of the larger sized damping holes is the worst. According to the results of the fluid flow characteristics at the same moment, when the spool is displaced to the medium opening position, the damping hole and the conical throttle valve no longer play a damping role. After a comprehensive comparative analysis, the differential high-flow safety valve assembled with *R*=2 mm damping holes has a relatively balanced pressure and velocity change and distribution of the fluid inside the flow path, with high stability of the fluid flow, and the right end of the centre hole and the area of the differential cavity will not have excessive pressure peaks. In the unloading process, not only can play a sufficient damping effect and can make the safety valve has a good working stability.

Analysis of the experimental results indicates that a damping hole radius of 2 mm provides optimal transient response characteristics and operational stability for differential large-flow safety valves. Based on this finding, the damping hole radius was standardized at 2 mm for subsequent production. All prototype valves manufactured subsequently maintained this 2 mm specification in their damping hole design.

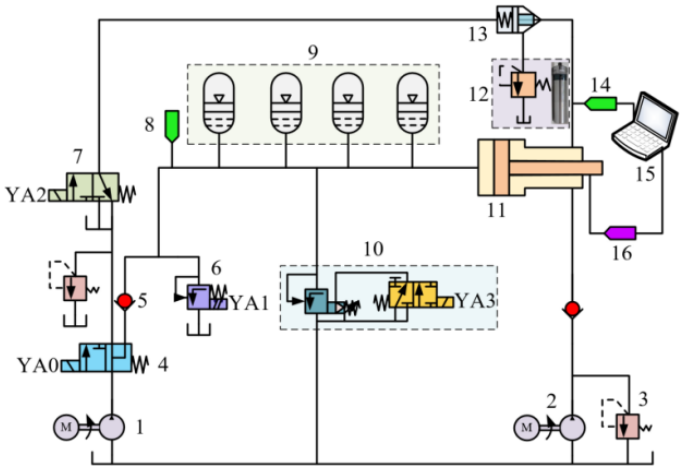

1. Main oil pump 2. Emulsion pump 3. Relief valve 4. Electromagnetic directional control valve 5. Check valve 6. Proportional relief valve 7. Switch valve 8. Pressure gauge 9. Energy storage tank 10. Relief valve 11. Pressure booster cylinder 12. Differential high-flow safety valve 13. Plug-in valve 14. Pressure sensor 15. Data acquisition computer 16. Displacement sensor

Fig. 25 Principle of rapid dynamic impact test system

4. EXPERIMENTAL STUDIES

The differential high-flow safety valve is designed to rapidly discharge pressure and reduce load during various impacts encountered in hydraulic various impacts, thereby protecting the column circuit. To evaluate the anti-impact performance of this valve, a rapid dynamic loading impact testing system was developed as shown in Fig. 25.

The working process of the rapid dynamic impact test system is divided into four stages: flushing, loading, testing and unloading:

Liquid Filling Phase: The emulsion pump 2 activates, directing the emulsion into the right chamber of the booster cylinder. As the pressure in the right chamber rises above that in the left chamber, it drives the piston to move leftward. The oil from the left chamber flows through the relief valve 10 into the reservoir. Position sensor 16 tracks the piston rod's displacement. When the displacement stabilizes, the liquid filling is complete, with pressure sensor 14 recording the final reading. The emulsion pump 2 then closes, while check valve 5 prevents backflow of emulsion from the right chamber of the booster cylinder.

Load stage: close the unloading valve 10, open the main oil pump 1, adjust the overflow valve 3, and the oil is injected into the accumulator 9 through the electromagnetic directional valve 4, check valve 5 and proportional overflow valve 6. The reading of the pressure gauge 8 gradually increases until the reading stabilizes to indicate the completion of loading.

Test Phase: Immediately halt the accumulator liquid charging process for closed solenoid directional control valve 4. Adjust proportional relief valve 6 to achieve system pressure meeting test requirements, while recording readings from displacement sensor 16 and pressure gauge 8. Activate switch valve 7 to discharge accumulator fluid, creating a pressure differential across the booster cylinder piston. A substantial volume of emulsion in the right chamber of the booster cylinder will be instantly discharged through the safety valve until pressure sensor 14 reading drops below the safety valve's activation threshold. Record readings from displacement sensor 16, pressure gauge 8, and pressure sensor 14 during this phase.

Unloading stage: After the test is completed, close the main oil pump 1. The system will discharge the oil in the left chamber of the pressurized cylinder to the hydraulic pump station through the unloading valve 10, and the pressure will gradually decrease to 0, that is, the unloading stage of the system is completed.

In accordance with the design requirements of the impact testing system, the main oil pump selected is a swashplate axial piston pump (model 63YCY14-1B) with a nominal pressure of 31.5 MPa and a displacement of 63 mL/r, using L-HM46 hydraulic oil as the working medium. The emulsion pump is a gear pump (model CBG2050) rated at 20 MPa nominal pressure, 25 MPa maximum pressure, and 50 mL/r displacement, utilizing 3%-5% emulsion as the working medium. The unloading valve employs a DBW-type pilot-operated relief valve from the 3X series, featuring a 10mm bore diameter, maximum flow rate of 200 L/min, and maximum operating pressure of 31.5 MPa.

In this paper, we use the NI PXIE 1042Q acquisition system, configured with the DAQ card model NI 6218, the input signal is 0-12 V, the pressure sensor model BP800, with a range of 0-70 MPa and an accuracy of 0.5% FS. The flow sensor model is JLLCB360 with a range of 1.6 m^3/h-360 m^3/h and an accuracy of 1.0% FS.

Based on the principles and structural composition of the impact testing system, a rapid dynamic loading impact test bench for differential high-flow safety valves was constructed, as shown in Fig. 26.

The dynamic pressure and flow characteristics of the differential high-flow safety valve at impact pressures of 56 MPa, 57 MPa, and 58 MPa are shown in Fig. 27.

As shown in Fig. 27, the safety valve was impacted at approximately 18.1ms relative time, causing rapid

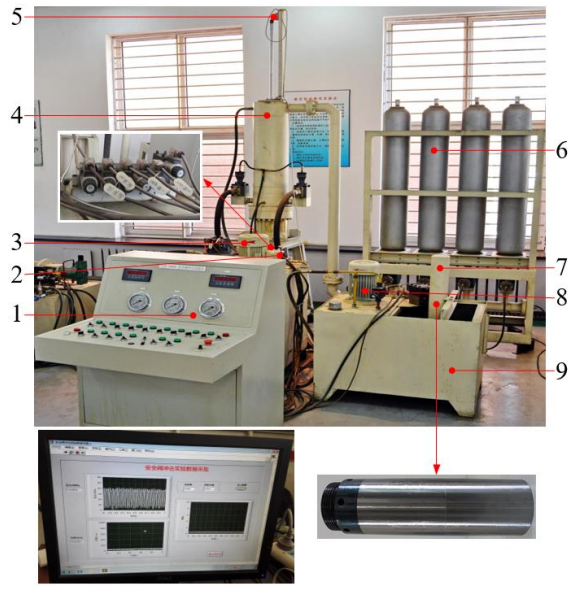

1. Control console 2. Pressure sensor 3. Main oil pump 4. Booster cylinder 5. Displacement sensor 6. accumulator 7. Tested safety valve 8. Emulsion pump 9. Oil tank

Fig. 26 Test site

pressure buildup. The impact pressure reached the safety valve's opening pressure value around 19.8 ms relative time, with a peak pressure of approximately 59.1 MPa occurring at 20.4 ms relative time. The pressure overshoot was about 18.2%, and after repeated fluctuations, the final stabilized value reached approximately 49.4 MPa. The relative time when stable unloading began was around 38.2 ms, with an unloading duration of approximately 4.8 ms. The flow fluctuation range ranged from 2792 L/min to 3898 L/min. During the stable unloading state, the flow fluctuations significantly decreased and ultimately stabilized at approximately 2996 L/min.As the impact pressure increased, the peak flow rate increased by 902 L/min.

As demonstrated in the analysis, the differential high-flow safety valve features a rated pressure and flow capacity of approximately 49.4 MPa and 2996 L/min respectively. With a maximum unloading flow rate of 3898 L/min and a valve core opening time under 2 ms, it can rapidly discharge high-pressure, high-flow shock loads from hydraulic support column circuits within 5 ms. The device demonstrates superior sensitivity with a pressure overshoot margin below 18.2%, validating its structural design rationality. Compared to conventional safety valves mentioned in the GB/T 25974.3-2010, this model exhibits enhanced rapid unloading performance and improved impact resistance capabilities.

5. CONCLUSION

This paper proposes a novel differential high-flow safety valve for hydraulic supports. By employing dynamic mesh technology and UDF functionality, we conducted simulation analysis on the transient fluid characteristics of the valve throughout its full working cycle with varying damping hole radii. A rapid dynamic loading impact test bench was subsequently established to evaluate the shock resistance performance of the

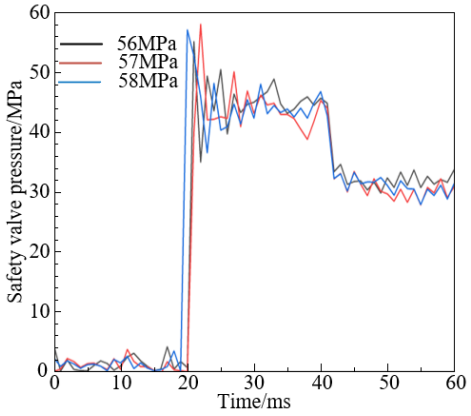

(a) pressure

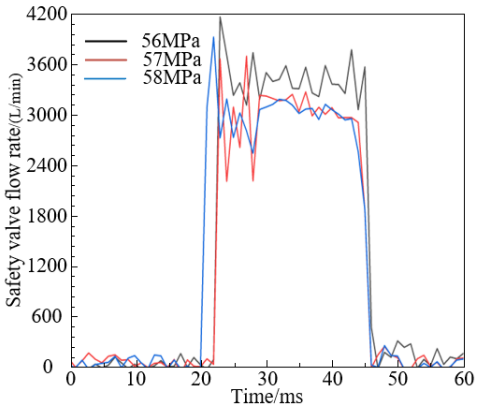

(b) flow rate

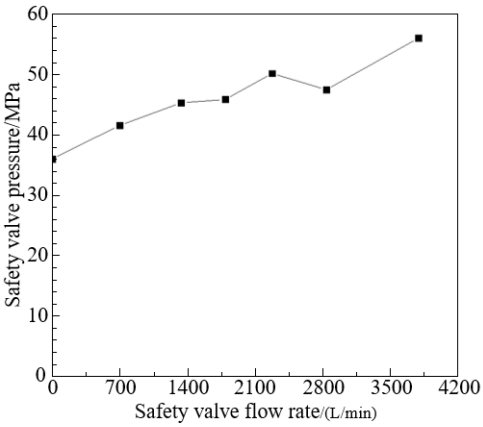

(c) P-Q

Fig. 27 Test results

optimized differential high-flow safety valve. The study primarily yields the following conclusions:

(1) As the differential large-flow safety valve's spool displacement increases, the peak flow velocity within the flow channel decreases, while the fluid pressure gradient distribution becomes more uniform, resulting in increased flow velocity at the outlet area. When the spool shifts to the small opening position, the conical throttle valve and damping hole exhibit maximum damping effects, with peak pressure values reaching their maximum at both the right end of the central orifice and the differential chamber region.

(2) When the radius of the damping hole is 2mm, the internal fluid pressure and velocity distribution of the differential large flow safety valve are relatively balanced, the fluid flow stability is higher, the pressure overshoot is lower, and the comprehensive performance of fluid transient characteristics and working stability is optimal.

(3) The rated flow and pressure of the designed differential large flow safety valve are about 2996 L/min and 49.4 MPa respectively, and the maximum unloading flow can reach 3898 L/min. The opening time of the valve core is less than 2 ms, the unloading time is less than 5ms, and the pressure overshoot is less than 20%, which proves that the safety valve has the performance of rapid unloading high pressure and large flow.

(4) The proposed novel safety valve structure achieves rapid unloading and shock resistance characteristics through pre-adjusted damping holes, however, the fixed configuration of these orifices during operation limits adaptive adjustment. Computational Fluid Dynamics (CFD) simulation employing the dynamic mesh method enables performance analysis of this new valve structure. This approach facilitates visualization of internal flow phenomena and provides guidance for structural improvements.

ACKNOWLEDGMENTS

This work was supported by the Liaoning Province Natural Science Foundation Joint Funding Program Projects (20240301, 20240318), the Scientific Research Project of Liaoning Provincial Education Department (LJ212510147029, JYTMS20230063)

CONFLICT OF INTEREST

The authors declare that they have no known competing financial interests or personal relationships that could have appeared to influence the work reported in this paper.

AUTHOR CONTRIBUTIONS

Li Nanqi: Conceptualization, Methodology, Investigation, Formal analysis, Data curation, Writing - original draft, Visualization; **Yang Xinle:** Conceptualization, Resources, Writing - review & editing, Supervision, Project administration, Funding acquisition; **Wang Sihan:** Methodology, Investigation, Validation, Data curation, Writing - review & editing; **Zhao Guochao:** Methodology, Software, Formal analysis, Validation, Writing - review & editing; **Song Yuning:** Investigation, Resources, Validation, Writing - review & editing.

REFERENCE

Burhani, M. G., & Hős, C. (2021). An experimental and numerical analysis on the dynamical behavior of a safety valve in the case of two-phase non-flashing flow. *Periodica Polytechnica Chemical Engineering, 65*(2), 251-260. https://doi.org/10.3311/PPch.16262

Chiavola, O., Frattini, E., & Palmieri, F. (2022). Performance Assessment of Hydraulic Micro Relief Valve. *Journal of Physics: Conference Series, 2385*(1), p. 012032. IOP Publishing. https://doi.org/10.1088/1742-6596/ 2385/1/012032

Couzinet, A., Gros, L., Pinho, J., Chabane, S., & Pierrat, D. (2014). Numerical modeling of turbulent cavitation flows in safety relief valves. *Pressure Vessels and Piping Conference, 46063*, V007T07A017. American Society of Mechanical Engineers. https://doi.org/10.1115/PVP2014-28384

Dasgupta, K., & Karmakar, R. (2002). Modelling and dynamics of single-stage pressure relief valve with directional damping. *Simulation Modelling Practice and Theory, 10*(1-2), 51-67 https://doi.org/10(1-2), 51-67.10.1016/s1569-190x(02)00059-x

Duan, H., Zhao, L., Yang, H., Zhang, Y., & Xia, H. (2022). Development of 3D top coal caving angle model for fully mechanized extra-thick coal seam mining. *International Journal of Mining Science and Technology, 32*(5), 1145-1152. https://doi.org/32(5), 1145-1152.10.1016/j.ijmst.2022.08.010

Filo, G., Lisowski, E., & Rajda, J. (2021). Design and flow analysis of an adjustable check valve by means of CFD method. *Energies, 14*(8), 2237. https://doi.org/10.3390/en14082237

Finesso, R., & Rundo, M. (2017). Numerical and experimental investigation on a conical poppet relief valve with flow force compensation. *International Journal of Fluid Power, 18*(2),111-122. https://doi.org/10.1080/14399776.2017.1296740

Hős, C. J., Champneys, A. R., Paul, K., & McNeely, M. (2014). Dynamic behavior of direct spring loaded pressure relief valves in gas service: Model development, measurements and instability mechanisms. *Journal of Loss Prevention in the Process Industries, 31*, 70-81. https://doi.org/31,70-81.10.1016 /j.jlp.2014.06.005

Kim, H., Kim, S., Kim, Y., & Kim, J. (2018). Optimization of operation parameters for direct spring loaded pressure relief valve in a pipeline system. *Journal of Pressure Vessel Technology, 140*(5), 051603. https://doi.org/10.1115/1.4040361

Liu, F., Wan, Z., Cao, S., Zhao, D., Liu, G., & Zhang, K. (2025). Fluid-structure interaction analysis on flow field and vibration characteristics of gas proportional valve. *Flow Measurement and Instrumentation, 101*, 102743. https://doi.org/10.1016/j.flowmeasinst.2024.102743

Morselli, S., Gessi, S., Marani, P., Martelli, M., & De Hieronymis, C. M. R. (2019, December). Dynamics of pilot operated pressure relief valves subjected to fast hydraulic transient. In *AIP Conference Proceedings* (Vol. 2191, No. 1, p. 020116). AIP Publishing LLC. https://doi.org/10.1063/1.5138849

Okabe, H., Tanaka, Y., Watanabe, A., Yoshida, F., Iio, S., & Haneda, Y. (2019, March). Cavitation in a spool valve for water hydraulics. In *IOP Conference Series: Earth and Environmental Science* (Vol. 240, No. 6, p. 062029). IOP Publishing. https://doi.org/10.1088/1755-1315/240/6/062029

Ren, B., Ding, K., Wang, L., Wang, S., Jiang, C., & Guo,

J. (2023). Research on an intelligent mining complete system of a fully mechanized mining face in thin coal seam. *Sensors, 23*(22), 9034. https://doi.org/10.3390/s23229034

Shan, P., Yan, Z., Lai, X., Xu, H., Hu, Q., & Guo, Z. (2024). An analytical methodology of rock burst with fully mechanized top-coal caving mining in steeply inclined thick coal seam. *Scientific Reports, 14*(1), 651. https://doi.org/10.1038/s41598-024-51207-3

Sharma, A. K., Kumar, N., & Das, A. K. (2023). Cavitation analysis in a re-designed direct acting pressure relief valve through flow visualization method. *Journal of Visualization, 26*(6), 1299-1319. https://doi.org/10.1007/s12650-023-00943-1

Xiangpeng, H., Xiaodong, J., Yang, L., & Yan, D. (2023). Study on instability mechanism of hydraulic support in downdip and updip coal face. *Alexandria Engineering Journal, 81*, 304-318. https://doi.org/10.1016/j.aej.2023.08.085

Zeng, Q., Ma, X., Wan, L., Zhu, Y., & Yue, Y. (2024). Research on the hydraulic support face guard mechanism and coupling characteristic of rib spalling in large mining heights. *Scientific Reports, 14*(1), 8110.https://doi.org/10.1038/s41598-024-58542-5

Zha, C., Pan, C., Sun, Z., & Liu, Q. (2024). Reliability sensitivity analysis for set pressure tolerance of the direct-operated relief valve in a vibration environment. *Journal of Mechanical Science and Technology, 38*(9), 4835-4845. https://doi.org/10.1007/s12206-024-0819-0

Zhao, G., Wang, H., Song, Y., & Zhang, C. (2020). Dynamic characteristics study on the two-stage safety valve used on hydraulic support under impact loading. *Journal of Theoretical and Applied Mechanics, 58*(3), 623-635. https://doi.org/10.15632/jtam-pl/116576